

THE CONNECTION BETWEEN X-RAY BINARIES AND STAR CLUSTERS IN NGC 4449

BLAGOY RANGELOV¹, ANDREA H. PRESTWICH², AND RUPALI CHANDAR¹

The Astrophysical Journal, in press

ABSTRACT

We present 23 candidate X-ray binaries with luminosities down to 1.8×10^{36} erg s⁻¹, in the nearby starburst galaxy NGC 4449, from observations totaling 105 ksec taken with the ACIS-S instrument on the *Chandra Space Telescope*. We determine count rates, luminosities, and colors for each source, and perform spectral fits for sources with sufficient counts. We also compile a new catalog of 129 compact star clusters in NGC 4449 from high resolution, multi-band optical images taken with the *Hubble Space Telescope*, doubling the number of clusters known in this galaxy. The *UBVI, H α* luminosities of each cluster are compared with predictions from stellar evolution models to estimate their ages and masses. We find strong evidence for a population of very young massive, black-hole binaries, which comprise nearly 50% of the detected X-ray binaries in NGC 4449. Approximately a third of these remain within their parent star clusters, which formed $\tau \lesssim 6-8$ Myr ago, while others have likely been ejected from their parent clusters. We also find evidence for a population of somewhat older X-ray binaries, including both supergiant and Be-binaries, which appear to be associated with somewhat older $\tau \approx 100-400$ Myr star clusters, and one X-ray binary in an ancient ($\tau \approx 10$ Gyr) globular cluster. Our results suggest that detailed information on star clusters can significantly improve constraints on X-ray binary populations in star-forming galaxies.

Subject headings: galaxies: individual (NGC 4449) — galaxies: star clusters — binaries: close — stars: evolution — X-rays

1. INTRODUCTION

Images of nearby starburst galaxies taken in X-rays with the *Chandra Space Telescope* are spectacular, showing a multitude of bright point sources. It is now generally accepted that most of these sources are high mass X-ray binaries (HMXBs) produced during recent star formation. HMXBs are binaries where one member of the system is a compact object, either a black hole or neutron star, and the other is a young, massive star. X-ray emission is produced as material is accreted from the young “donor” star onto the compact object. HMXBs can be divided into two general categories based on the type of donor star: 1) a Be star (Be/X-ray binary), or 2) a supergiant star (SG/X-ray binary).

Previous studies have suggested an intriguing connection between HMXBs and young stellar clusters: many of the former are found close to, but not coincident with, young star clusters. These observations are broadly consistent with a scenario where X-ray binaries (XRBs) form in star clusters, but have sufficiently large velocities that they are expelled from their parent cluster (Zezas et al. (2002), Kaaret et al. (2004)). There are three mechanisms that might displace HMXBs from their birthsites. The binary could be given a “kick” during an asymmetric supernova explosion that forms the black hole or neutron star, or it could be ejected via dynamical interactions with other stars in a dense cluster core (McSwain et al. 2007). A third scenario that could explain the observed spatial displacement between HMXBs and young star clusters is that X-ray binaries formed in clusters that

have since dispersed.

In this paper, we investigate the relationship between HMXBs and star clusters using the best X-ray and optical observations currently available for the starburst galaxy NGC 4449. We analyse observations taken with the *Chandra Space Telescope* to select X-ray binaries in NGC 4449, and optical images taken with the *Hubble Space Telescope* (*HST*) to detect star clusters and to estimate their ages and masses. An optical color image of NGC 4449 based on the *HST* images is shown in Figure 1. Our primary goals are to constrain the nature of X-ray binaries and in particular HMXBs, and to explore the relationship between HMXBs and star clusters in NGC 4449.

The rest of this paper is organized as follows. In Section 2 we present the X-ray observations from *Chandra*, including data reduction, source detection and some basic models used for interpretation. In Section 3 we present the optical observations from the *HST* and a new catalog of compact star clusters, including their integrated colors and luminosities, and we derive their masses and ages. The mass and age distributions of the clusters and what they tell us about the formation and disruption of the clusters are the subject of Section 4, while Section 5 presents the spatial correlation between the clusters and the candidate HMXBs. Section 6 synthesizes these results to constrain the nature of the HMXBs in NGC 4449, and Section 7 summarizes the main results of this work.

2. X-RAY OBSERVATIONS FROM CHANDRA

NGC 4449 is an irregular, star-forming galaxy located at a distance of 3.82 ± 0.27 Mpc (Annibali et al. 2008). With an integrated magnitude of $M_B = -18.2$ it is somewhat more luminous than the Large Magellanic Cloud

blagoy.rangelov@gmail.com

¹Department of Physics & Astronomy, The University of Toledo, 2801 West Bancroft Street, Toledo, OH 43606

²Harvard-Smithsonian Center for Astrophysics, 60 Garden Street, Cambridge, MA 02138

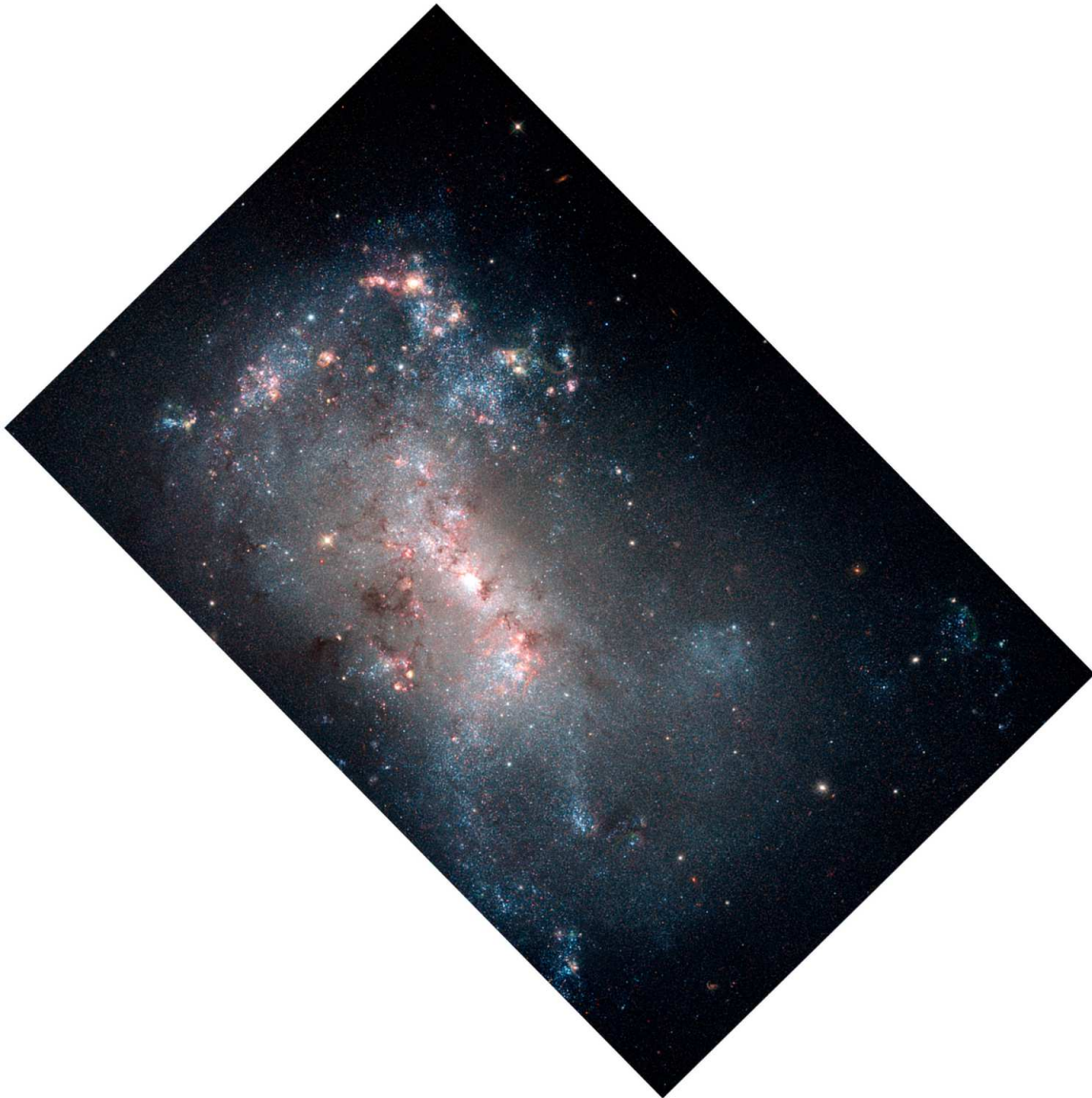


Figure 1. Color image of NGC 4449 produced using the *HST*/ACS observations described in Section 3. The F435W ($\approx B$ band) image is shown in blue, the F555W ($\approx V$ band) image in green, and the red image combines the F814W ($\approx I$ band) and F658N (H_α) filters. North is up and east is to the left. This image is $5'$ along the long side. (Credit: NASA, ESA, A. Aloisi (STScI/ESA), and The Hubble Heritage (STScI/AURA)-ESA/Hubble Collaboration)

(Hunter 1997). NGC 4449 has a current star formation rate of $\approx 1.5 M_\odot \text{ yr}^{-1}$ (Thronson et al. 1987) and a near-solar present-day gas abundance ($12 + \log[O/H] = 8.83$; Grevesse & Sauval (1998)).

2.1. Data and Reduction

We use three sets of archival *Chandra* observations of NGC 4449, with integration times of 30 ksec (ObsID: 2031, PI: Heckman), 15 ksec (ObsID: 10125, PI: Long), and 60 ksec (ObsID: 10875, PI: Long), to detect X-ray point sources in NGC 4449. Basic information for the three sets of observations is given in Table 1. The data were taken with the Advanced CCD Imaging Spectrometer (ACIS) instrument on the *Chandra* telescope on February 4, 2001 in “faint” mode (ObsID: 2031), and March 4 and 7, 2010 in “vfaint” mode (ObsIDs: 10125 and 10875). The galaxy was positioned on the

back-illuminated S3 CCD chip. We processed the data using the *Chandra* Interactive Analysis of Observations (CIAO) software (version 4.2) and *Chandra* Calibration Data Base (CALDB) version 4.3.0³, and restricted the data to the energy range between 0.3-8 keV. The observations were filtered in three energy bands – 0.3-1 keV (soft), 1-2 keV (medium) and 2-8 keV (hard).

2.2. Source Detection and X-ray Properties

We use CIAO’s Mexican-hat wavelet source detection routine *wavdetect* (Freeman et al. 2002) to create source lists. Wavelet scales of 1.4, 2, 4, 8, and 16 pixels and a detection threshold of 10^{-6} were used, which typically results in 1 spurious detection per million pixels. The output sources were examined visually to verify each de-

³ <http://cxc.harvard.edu/ciao/>

Table 1
Chandra observations

ObsId	Date	PI	Exposure (ks)
2031	2001-02-04	Heckman	30
10125	2009-03-04	Long	15
10875	2009-03-07	Long	60

tection, and to correct the source catalog when multiple detections occurred. A catalog of X-ray point sources detected in the *Chandra* observations is presented in Table 2, and the locations of these sources are shown in Figure 2.

A number of measurements and estimates are made for each source – total number of counts and the counts measured in the soft, medium, and hard energy bands. We calculate two X-ray colors, a “soft” color defined as $H1 = (M - S)/T$, and a “hard” color defined as $H2 = (H - M)/T$, where S , M and H are the total counts measured in the soft, medium and hard bands (Prestwich et al. 2003), and T is the total number of counts in all three bands. The luminosity of each source is estimated by fitting its spectrum with a power law model with a photon index $\Gamma = 1.5$. These values are compiled in Table 2.

There are eleven sources which have sufficient counts (> 50) for a crude spectral fit. We were able to fit ten of these with simple X-ray spectral models, as summarized in Table 3. One source, X15, is in a region with high background from diffuse emission and we were unable to obtain a satisfactory fit. X-ray spectra and responses (including sensitivity of the instrument and CCD) were extracted using standard CIAO software. Spectra were grouped for a minimum of 15 counts per bin. The fits were performed using XSPEC V 12.0 over an energy range 0.2–8.0 keV. For each source, we tried three models: a simple power law (PL), a MEKAL model⁴, and a multi-color disk (MCD⁵) model. A fixed foreground Galactic column $n_H = 1.5 \times 10^{20} \text{ cm}^{-2}$ was assumed in each fit. The fits allow for an additional variable column due to absorption intrinsic to the source. The best fit model and parameters for each source are given in Table 3. Observed X-ray fluxes and estimated luminosities were calculated for the 0.3 – 8 keV energy range (both uncorrected for absorption) using the best fit parameters in the table.

2.3. X-ray Colors and Models

After examining the resulting X-ray source catalog, we eliminate some sources from further consideration in this work for the following reasons. First, we remove all sources located beyond the optically luminous portion of NGC 4449 ($R \sim 3\text{--}4 \text{ kpc}$), since these are almost certainly background galaxies and not associated with NGC 4449 itself. We also eliminate one source

⁴ An emission spectrum from hot diffuse gas, e.g. Liedahl et al. (1995)

⁵ A superposition of multi-temperature blackbody spectra expected from optically-thick accretion disk; the model only constrains the temperature of the inner disk T_{in} , e.g. Mitsuda et al. (1984)

Table 2
X-ray source catalogue

ID	RA	DEC	Soft Color	Hard Color	L_X^1 (erg s^{-1})
X8	187.00308	44.07569	0.20	0.00	4.55E+36
X14	187.00572	44.09145	0.15	-0.50	9.41E+36
X18	187.01634	44.09551	0.01	-0.09	7.68E+37
X13	187.02855	44.09120	0.31	-0.42	9.21E+36
X6	187.02988	44.07074	0.34	0.14	1.47E+37
X29	187.03043	44.12264	0.04	-0.07	3.34E+37
X10	187.03065	44.08164	-0.33	-0.16	5.67E+37
X12	187.03891	44.08566	-0.06	-0.32	3.01E+38
X20	187.04055	44.09808	0.23	-0.13	1.01E+38
X11	187.04576	44.08327	0.34	-0.26	3.05E+36
X23	187.04671	44.11066	-0.24	-0.26	2.25E+37
X15	187.04985	44.09188	-0.44	-0.04	7.66E+37
X24	187.04997	44.11149	0.02	-0.29	5.81E+37
X21	187.05013	44.09955	-0.28	-0.25	1.19E+37
X28	187.05533	44.11557	-0.01	-0.32	6.93E+37
X31	187.06829	44.12765	-0.08	0.41	9.53E+36
X22	187.07433	44.10939	0.41	-0.13	8.59E+38
X19	187.07917	44.09585	-0.90	-0.02	2.01E+37
X41	187.04336	44.09946	-1.00	0.00	1.43E+37
X42	187.06327	44.08829	-0.41	-0.57	1.78E+36
X43	187.08341	44.10589	0.41	0.09	3.36E+36
X44	187.05553	44.11308	0.13	0.09	1.13E+36
X46	187.04041	44.08867	-0.20	-0.23	7.59E+36
X26 ²	187.04569	44.11343	0.11	-0.35	2.57E+38

¹ X-ray luminosities (0.3 – 8 keV range) are derived by fitting a power law ($\Gamma = 1.5$) to the data. An assumed Galactic $n_H = 1.5 \times 10^{20} \text{ cm}^{-2}$ is applied.

² Supernova remnant.

that is a confirmed supernova remnant in NGC 4449 (Patnaude & Fesen 2003), and another which appears to be a spurious detection of diffuse emission near the center of the galaxy. Two additional X-ray sources are coincident with foreground stars and were also eliminated. Our final catalog contains 23 sources that we believe are X-ray binaries. These are listed in Table 2.

The observed H1 vs. H2 colors of the X-ray binaries are shown in Figure 3. Two models are shown for reference. The red line shows predictions from disk blackbody models with temperatures ranging from 0.1 – 1.0 keV. Black hole binaries typically have disk blackbody temperatures of $kT \sim 1.0 \text{ keV}$. The orange line shows the effect of adding absorption to the disk blackbody models. The green line represents a power law with increasing photon index from 1.0 – 3.0. Accreting low mass neutron star binaries typically have absorbed power law spectra with photon index ~ 2.0 . Figure 3 suggests that NGC 4449 has a mix of X-ray binary populations typical of a galaxy that has had on-going star formation, with some sources better following disk black-body models and others in the absorbed portion of the diagram. The nature of the X-ray binaries will be discussed in more detail in Section 6.

3. OPTICAL OBSERVATIONS FROM *HST*

It has been suggested that the dense environments found in compact star clusters may be very efficient in producing XRBs (e.g., McSwain et al. (2007)). Regardless of whether or not XRBs form within compact clusters, the clusters are good tracers of star formation in galaxies, and hence can provide important constraints on the XRB population. The goals of this section are

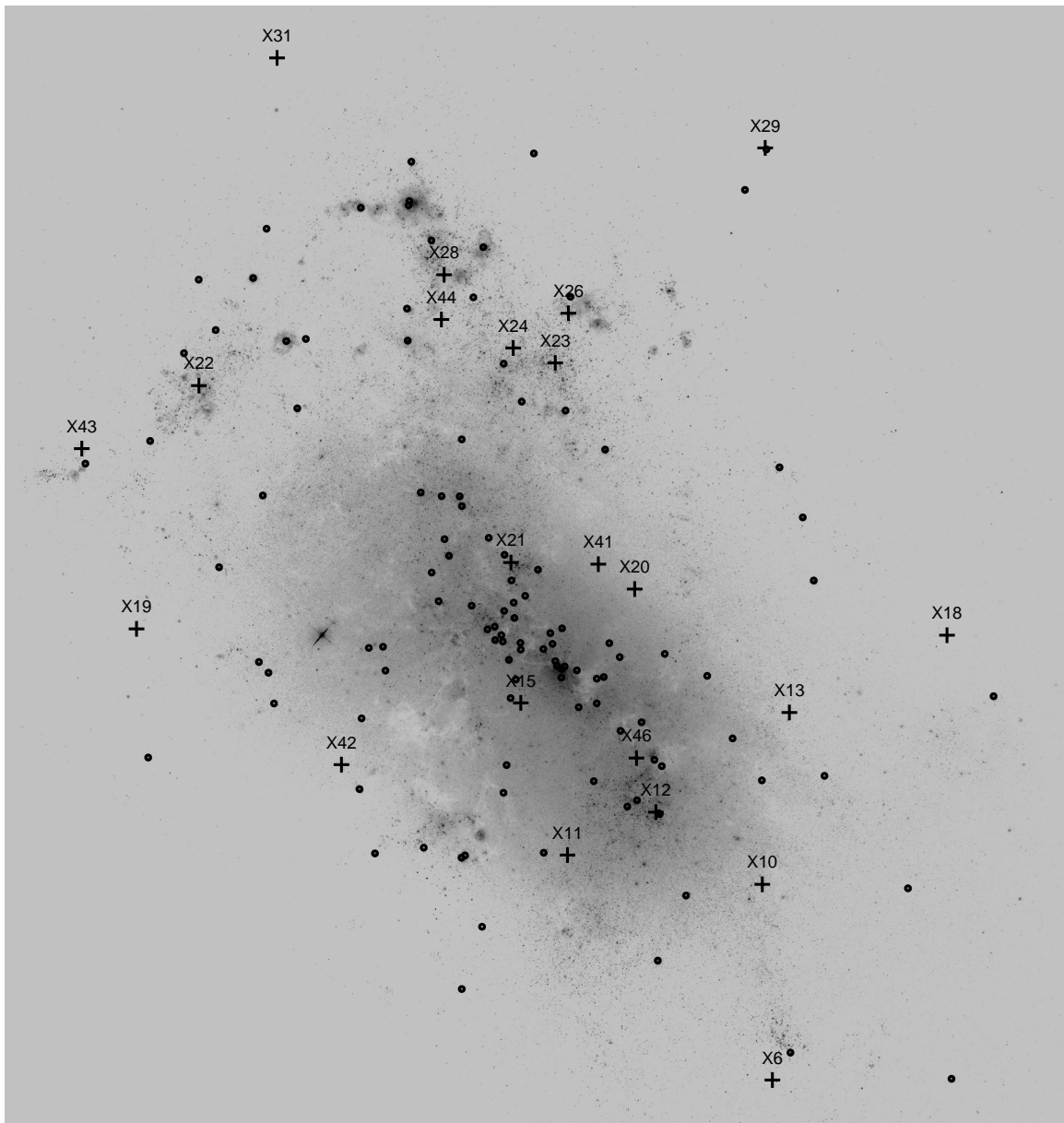


Figure 2. V band (F555W filter) image of NGC 4449 taken with the ACS camera on the *HST*. North is up and east is to the left. The locations of star clusters selected from optical *HST* images are shown as circles. The locations of X-ray sources selected from *Chandra* X-ray observations are labeled and shown as crosses.

two-fold: (1) select a new catalog of compact star clusters in NGC 4449, to correlate with the locations of the XRBs, and (2) measure luminosities and colors for any point source coincident with an XRB and hence likely to be the donor star (discussed in Sections 5.2 and 6.4). While a catalog of clusters in NGC 4449 already exists (Gelatt, Hunter & Gallagher 2001), it is based on partial imaging taken with the WFPC2 instrument on board *HST*, and there are now deeper, higher resolution data with full coverage of NGC 4449 available from the Wide Field Channel (WFC) camera of the Advanced Camera for Surveys (ACS) instrument.

3.1. Data and Photometry

ACS/WFC imaging of two positions within NGC 4449 was taken in the F435W ($\approx B$), F555W ($\approx V$ band),

F814W ($\approx I$ band), and the F658N ($H\alpha$) filters, on November 10-11, 2005 (Proposal ID GO: 10585, PI: Aloisi). Four individual exposures were taken in each filter at each pointing. The ACS/WFC has a pixel scale of $0.''049$, or a projected scale of 18.4 pc per arcsecond at the assumed distance of 3.82 ± 0.27 Mpc (Annibali et al. 2008) to NGC 4449. We downloaded the ACS data from the Hubble Legacy Archive⁶ (HLA). The HLA combines the individual flatfielded exposures for a specific filter together using the PYRAF task *Multidrizze*, and outputs geometrically corrected images. For the NGC 4449 observations, the HLA used stars from the U.S. Naval Observatory catalogue to astrometrically correct the images.

⁶ <http://hla.stsci.edu/>

Table 3
Model parameters for X-ray sources with > 50 counts

ID	Net Counts	Best Fit Model	n_H ($\times 10^{22} \text{ cm}^{-2}$)	Photon index	T_{in}^1 (keV)	T^2 (keV)	χ^2 / d.o.f.	Flux ³ ($\text{erg s}^{-1} \text{ cm}^{-2}$)	L_X^3 (erg s^{-1})
X18	141.3	ABS*PL	$(4.5^{+8.0}_{-4.0}) \times 10^{-2}$	1.5 ± 0.3	—	—	2.4 / 7	3.65E-14	6.30E+37
X29	84.8	ABS*PL	$(2.2^{+12.5}_{-2.2}) \times 10^{-2}$	$1.26^{+0.6}_{-0.4}$	—	—	0.43 / 3	2.48E-14	4.30E+37
X10 ^a	172.7	ABS*(PL+MEKAL)	$(9.5^{+40}_{-9.0}) \times 10^{-3}$	2.1 ± 0.4	—	$0.46^{+0.16}_{-0.4}$	7.0 / 7	2.72E-14	4.70E+37
X12	1197.7	ABS*MCD	$(4.0^{+4.0}_{-8.5}) \times 10^{-3}$	—	0.60 ± 0.5	—	85.9 / 71	1.58E-13	2.76E+38
X20	201.4	ABS*PL	0.19 ± 0.1	$1.7^{+0.4}_{-0.3}$	—	—	13.72 / 11	4.80E-14	8.35E+37
X23 ^b	106.0	ABS*MCD	$0.037^{+0.2}_{-0.04}$	—	0.37 ± 0.13	—	5.28 / 4	1.13E-14	1.95E+37
X24	186.8	ABS*PL	$0.19^{+0.06}_{-0.08}$	$2.4^{+0.4}_{-0.3}$	—	—	7.54 / 10	3.20E-14	5.66E+37
X21	58.9	ABS*MCD	$0.21^{+0.38}_{-0.08}$	—	0.23 ± 0.1	—	2.89 / 2	6.00E-15	1.68E+37
X28 ^a	309.8	ABS*MCD	$0.04^{+0.04}_{-0.03}$	—	0.64 ± 0.1	—	24.7 / 17	3.98E-15	6.98E+37
X22	1411.6	ABS*PL	0.6 ± 0.07	$1.9^{+0.16}_{-0.14}$	—	—	86.73 / 85	4.34E-13	7.62E+38

¹ The inner temperature of the multi-color disk model.

² MEKAL model temperature.

³ Observed X-ray fluxes and estimated luminosities for the 0.3 – 8 keV energy range, uncorrected for absorption.

^a Possible line emission.

^b Excess flux just over 1 keV.

Table 4
HST Images

<i>HST</i> Instrument	Proposal ID	Filter	Exposure time (s)
WFPC2	6716	F336W	2×520
ACS/WFC	10585	F435W	4×3660 (PosA)
			4×3478.91 (PosB)
		F555W	4×2460
		F658N	4×360
		F814W	4×2060

We also use available F336W ($\approx U$) band imaging of two pointings within NGC 4449, taken with the WFPC2 camera (Proposal ID GO: 6716, PI: Stecher). Each position has two exposures. The WFPC2 has four CCDs – the Planetary Camera (PC) has a scale of $0.''0456 \text{ pix}^{-1}$, and the three Wide Field (WF) CCDs have a scale of $0.''0996 \text{ pix}^{-1}$. Note that there are two sets of images for each WFPC2 observation available in the HLA: a combined WFPC2 image including all four CCDs with the PC resampled to the same resolution as the three WF CCDs, and an image of only the PC, at its original pixel scale. We have used the combined WFPC2 image when our cluster candidates were in one of the three WFs and WFPC2-PC for objects located in the PC. Details on pointings and exposure times for the *HST* data used here are given in Table 4.

We identified $\sim 200,000$ sources in each ACS pointing (in the *V* band), using the IRAF⁷ DAOFIND task. These include star clusters and bright, individual stars in NGC 4449, as well as some foreground stars and background galaxies. We perform circular aperture photometry of all detected sources using radii of 1 and 3 pixels and background annuli of 8 and 13 pixels, using the PHOT task in IRAF. We use zeropoints on the VEGAMAG system taken from Table 9 in Holtzman et al. (1995a)

⁷ IRAF is distributed by the National Optical Astronomy Observatories, which are operated by the Association of Universities for Research in Astronomy, Inc., under cooperative agreement with the National Science Foundation.

for the WFPC2/F336W filter, and from Table 10 in Sirianni et al. (2005) for the ACS observations. Corrections for inefficiency in the charge transfer were determined for the WFPC2/F336W photometry based on the formulae given by Dolphin (2000; we have used the most recent characterization available from A. Dolphin’s website <http://purcell.as.arizona.edu/wfpc2.calib/>). We also applied aperture corrections to extrapolate from our fixed aperture radius to the total magnitude in each filter, based on the concentration index (*CI*, the magnitude difference measured between a radius of 1 and 3 pixels) measured for each source. We obtained a linear fit between the measured *CI* and aperture corrections for ≈ 20 hand-selected, relatively isolated sources, and used this fit to estimate the aperture corrections for the rest of the sources.

3.2. Color Magnitude Diagram of Donor Stars

The colors and luminosities of individual stars give an estimate of their masses and hence a constraint on their ages. In several cases, the optical images reveal a single point source within the positional uncertainty of an XRB, which is likely the donor star. Although a full analysis of the spectral energy distributions for these stars is beyond the scope of this paper and will be presented in a future work, we can use our photometry to broadly assess their ages. In Figure 4, we compare the measured luminosities and colors for these matched optical sources with solar metallicity stellar isochrones with ages of 10 Myr, 100 Myr, and 1 Gyr from the Padova group (Girardi et al. (2008); Marigo et al. (2008)). These provide a rough guide to the ages/types of the candidate donor stars, and suggest that the bright stellar sources associated with X10 and X24 are supergiant stars, while those associated with X6, X31, and X14 are significantly fainter and hence may be somewhat older.

3.3. Cluster Selection

We measure the sizes of all detected objects using the *Ishape* software (Larsen 1999). This gives a better measure than *CI* of the sizes of relatively bright, isolated star

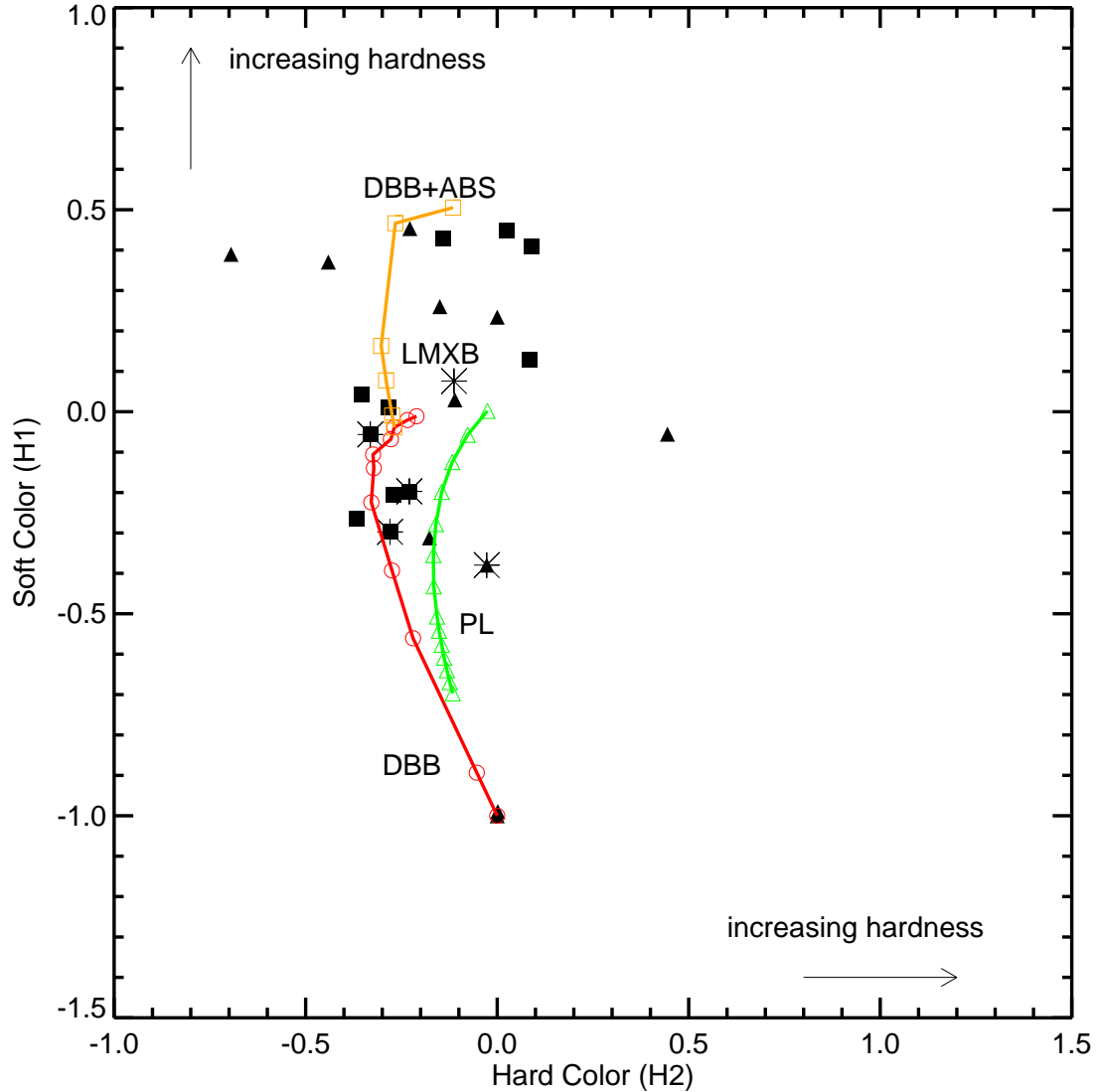


Figure 3. X-ray color-color diagram of X-ray binaries in NGC 4449. The H1 and H2 colors are defined in Section 2. Candidate high mass black hole binaries are shown as squares, and the rest of the sample is shown as triangles. The asterisks show the X-ray sources that are coincident with clusters. Theoretical tracks are shown as the open symbols connected with solid lines. The green triangles represent a power law (PL) with an increasing photon index from 1.0 to 3.0, and the red circles show predictions for diskblack-body models (DBB) with increasing temperature from 0.1 to 1.0 keV. The orange squares are a disk black-body model with $T=0.9$ keV and an increasing hydrogen column density (DBB+ABS) n_H in steps of $0, 1 \times 10^{20}, 5 \times 10^{20}, 1 \times 10^{21}, 5 \times 10^{21},$ and $1 \times 10^{22} \text{ cm}^{-2}$. See text for details.

clusters. *Ishape* convolves analytic profiles with the PSF, and determines the best fit to each source. We assume a KING30 profile, a single mass King (1966) model with a fixed ratio of tidal to core radius of 30 and fit the data within a radius of 5 pixels. For more details on *Ishape* and estimating the sizes of clusters, see Larsen (1999).

Most star clusters are slightly broader than the PSF at the distance of NGC 4449. The biggest challenge in selecting compact star clusters from the entire source list is to separate them from chance blends and superpositions in the crowded star forming regions. We use the following criteria to select star cluster candidates: (1) $m_V \leq 22$ ($M_V \approx -6$ at the assumed distance of 3.82 Mpc for NGC 4449); (2) $CI > 1.3$; (3) $\text{FWHM} > 0.2$ pixels, i.e. at least 0.2 pixels broader than the PSF, as measured by *Ishape*; and (4) no “neighbors”, i.e. other

object detected within a 5 pixel radius. A final by-eye inspection was made to throw out some remaining blends (at the $\approx 20 - 30\%$ level). The final catalog contains 129 candidate star clusters, double the number published previously by Gelatt, Hunter & Gallagher (2001). Basic information for the selected clusters, including their locations and measured photometry, is given in Table 5. The cluster locations are shown in Figure 2.

3.4. Cluster Age, Mass and Size Estimates

Figure 5 compares predictions from solar metallicity stellar population models of Charlot & Bruzual (2007; hereafter CB07, private communication; see also Bruzual & Charlot (2003)), with colors measured for our final cluster sample. Crosses mark the predicted colors for $10^6, 10^7, 10^8, 10^9,$ and 10^{10} yr clusters, starting from

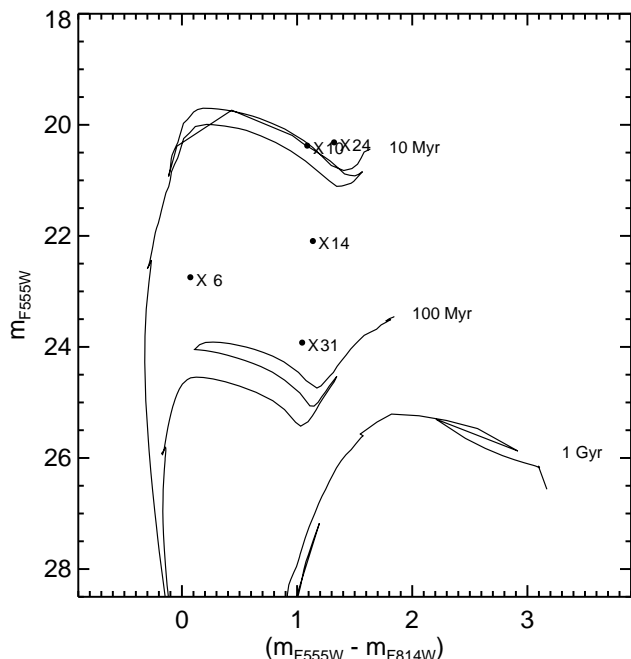


Figure 4. Color magnitude diagram of optical point sources which are unique counterparts to X-ray sources. The solid lines are Padova isochrones (for $Z = 0.02$) of 10 Myr, 100 Myr and 1 Gyr (from left to right).

Table 5
Star cluster catalogue

Number	RA	DEC	$U-B$	$V-I$	Age ¹ $\log(\tau/\text{yr})$
1	187.05396	44.083114	-2.106	-0.295	6.40
2	187.05370	44.083248	-2.195	-0.395	6.02
3	187.06067	44.083354	-0.303	1.080	9.30
...					

Note. — This table is published in its entirety in the electronic edition of the *Astrophysical Journal*. A portion is shown here for guidance regarding its form and content.

¹ Typical uncertainties are approximately ± 0.3 in $\log \tau$.

the upper left. The arrow shows the direction of reddening for a Galactic-type extinction law (Fitzpatrick 1999).

The model predictions match our cluster photometry relatively well. The majority of the clusters have blue integrated colors, indicating that they are fairly young, with ages $\tau \lesssim \text{few} \times 10^8$ yr. At the top of the diagram there are a few young clusters in crowded regions that fall above the models, likely due to some contamination from neighbors in the lower resolution U band images (we see a similar effect for the colors of clusters in M51; Chandar et al. (2010a)). The few sources with $U-B$ colors significantly redder than the model predictions are somewhat faint in the U band, leading to large uncertainties in this color. The bottom panel of Figure 5 shows the $B-V$ vs. $V-I$ two-color diagram, and includes some objects for which no U band photometry was measured, either because they are outside the field of view or because they are too faint in this band. The sources which fall significantly below (redward of) the model predictions in $B-V$ have strong nebular line emission (which is observed in the narrow-band F658N

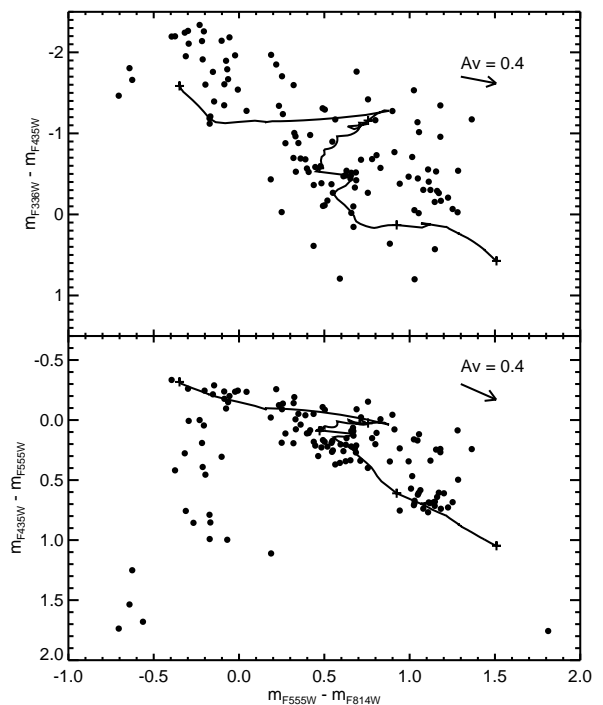


Figure 5. Optical two-color diagrams of all star clusters in our sample. The solid line shows predictions from the single stellar population models of CB07 and the crosses show the following predicted ages: $\log(\tau/\text{yr}) = 6, 7, 8, 9$ and 10 , starting from the upper-left. The arrow shows the direction of reddening.

($H\alpha$) filter), moving them off the model track. While two-color diagrams like those shown in Figure 5 are useful for visualizing the evolution of clusters, we actually use a χ^2 minimization technique to estimate the ages of the clusters. This means that points outside the models (e.g., the “high” points in Figure 5) can be reasonably well fit.

We estimate the age τ and extinction A_V for each cluster as we have done in previous works (see e.g., Fall et al. (2005) for details), by performing a least χ^2 fit comparing observed magnitudes with the predictions from the CB07 stellar population models with solar metallicity ($Z = 0.02$), which appear to match the measured colors of clusters in NGC 4449 reasonably well. The best fit combination of τ and A_V for each cluster returns the minimum χ^2 : $\chi^2(\tau, A_V) = \sum_{\lambda} W_{\lambda} (m_{\lambda}^{\text{obs}} - m_{\lambda}^{\text{mod}})^2$, where the sum runs over all available broad-band ($UBVI$) filters and the F658N narrow-band filter, but requires a minimum of three measurements (including the V band) to estimate age and extinction. The weights W are related to the photometric uncertainty σ_{λ} as $W_{\lambda} = [\sigma_{\lambda}^2 + (0.05)^2]^{-1}$. The F658N filter includes both stellar continuum and nebular line emission, and is dominated by line emission from ionized gas for the youngest ($\tau \lesssim \text{several} \times 10^6$ Myr) objects, and by continuum emission from stars for clusters with ages of $\tau \gtrsim 10^7$ yr. This enables us to use the narrow-band filter as a fifth data point in many cases, regardless of the age of the cluster.

We tested our method by estimating ages and masses from our χ^2 analysis for different assumptions regarding

extinction and by comparing our photometry with the predictions from a model with lower metallicity ($Z = 0.008$). In general, we find that the age estimates are quite robust for very young clusters ($\tau \lesssim 6 \times 10^6$ yr) that have nebular emission, and for clusters with ages between 3×10^7 yr $\lesssim \tau \lesssim 10^9$ yr. Clusters older than $\approx 10^9$ yr suffer from the well-known age-metallicity degeneracy, and we cannot tell if they are approximately a Gyr or older than ≈ 10 Gyr from the data presented here. Eleven clusters in our catalog have integrated colors similar to those of metal-poor globular clusters in our Galaxy (and in many other galaxies) with $0.8 \leq V - I \leq 1.3$ and $0.6 \leq B - V \leq 0.9$. The dating of clusters with no nebular emission and with ages between $\approx 6 \times 10^6$ yr and $\approx 3 \times 10^7$ yr is degenerate in some cases, with two nearly equally good combinations of age and extinction. We estimate that typical uncertainties are ≈ 0.3 in $\log \tau$ for clusters with $\tau \lesssim 10^9$ yr, typical for this method (e.g., Fall et al. (2009)).

The mass of each cluster is estimated from the total V band luminosity, corrected for extinction, and the age-dependent mass-to-light ratios (M/L_V) predicted by the CB07 models.

4. FORMATION AND DISRUPTION OF THE CLUSTERS

The mass and age distributions of a population of star clusters provides important clues to the formation and disruption of the clusters. In Figure 6 we show the mass and age estimates for star clusters in NGC 4449. The solid line represents $M_V = -7$, the approximate completeness limit of our sample, and shows that our sample does not contain clusters over the same mass range at all ages, because clusters fade over time. The mass-age diagram shows some small scale features, such as a sparsely populated region in the range $7.0 \lesssim \log(\tau/\text{yr}) \lesssim 7.6$ yr. This particular feature occurs where the predicted colors loop back on themselves, covering a small region in color space over a relatively long time, and effectively resulting in a gap. This artificial, empty stripe and similar features do not affect our conclusions.

Qualitative trends in the distribution of cluster ages and masses are apparent from the mass-age diagram. We see that NGC 4449 has formed relatively massive clusters ($M \gtrsim 10^4 M_\odot$) more or less continuously over the last 10^9 yr. A number of clusters (approximately half of our sample), formed very recently, in the last $\tau \lesssim 10^7$ yr, and a number of clusters clearly formed $\approx 1 - 3 \times 10^8$ yr ago. As mentioned in Section 3.3, our sample includes ≈ 11 candidate ancient globular clusters, implying that NGC 4449 began forming stars approximately a Hubble time ago. This is broadly consistent with the results of Annibali et al. (2008), who found that stars in NGC 4449 have formed over at least the last $\approx 10^9$ yr, with tentative evidence for earlier star formation as well, based on the colors and luminosities of individual stars. Qualitatively, the overall distribution of cluster ages and masses in NGC 4449 appears to be similar to that in other galaxies with very different environments and star formation histories, such as the merging Antennae galaxies (e.g., Fall et al. (2005), and the more quiescent Magellanic Clouds (Chandar et al. 2010a), although the gap

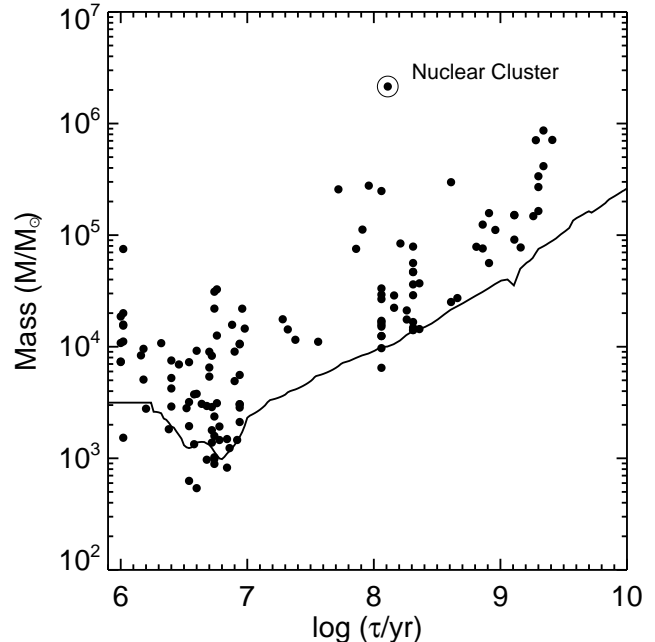


Figure 6. Mass-age diagram of all clusters in our sample. The solid line shows the approximate magnitude limit of $M_V = -7.0$.

between $10^7 - 10^8$ yr is somewhat more prominent. We present a more quantitative analysis below.

Figure 7a shows the age distribution for clusters in NGC 4449 in two different intervals of mass. Note that the data points for each distribution are restricted to a mass-age range that is not affected by incompleteness (i.e. above the solid line), so the observed shapes are caused by the formation and disruption of the clusters and not by their fading out of our sample. Although there are few data points, these distributions appear to decline steeply, and can be approximated by a simple power law, $dN/d\tau \propto \tau^\gamma$, with best fits of $\gamma = -0.91 \pm 0.13$ for clusters more massive than $2 \times 10^4 M_\odot$, and $\gamma = -1.21 \pm 0.21$ for clusters with masses between $1 - 2 \times 10^4 M_\odot$. These values of γ are the same within the uncertainties. We find that γ can change by up to ≈ 0.3 if different bin sizes and centers are used, but the overall decline starting at very young ages does not change. Based on these experiments, we take $\gamma = -1.0 \pm 0.3$.

Figure 7b shows the mass function for clusters in NGC 4449 in two different intervals of age. These mass functions can be approximated by a power law, $dN/dM \propto M^\beta$, with best fit values of $\beta = -2.25 \pm 0.15$ for $\tau < 10^7$ yr, and $\beta = -2.07 \pm 0.19$ for $\tau = 1 - 2 \times 10^8$ yr, which are the same within the uncertainties. We take β to be -2.16 ± 0.3 , the mean and range of the values above.

Because the mass and age distributions appear to be at least approximately independent of one another, the joint distribution of cluster ages and masses $g(M, \tau)$ can be approximated as $g(M, \tau) \propto M^\beta \tau^\gamma$, with $\beta \approx -2$ and $\gamma \approx -1$, for $\tau \lesssim \text{few} \times 10^8$ yr and $M \gtrsim 10^4 M_\odot$, similar to the form observed for clusters in the Magellanic Clouds (Chandar et al. 2010a), M83 (Chandar et al. 2010b), and in the Antennae (Whitmore et al. 2007; Fall et al. 2010).

Chandar et al. (2010c) compiled results for the age distribution of star clusters in over a dozen different galax-

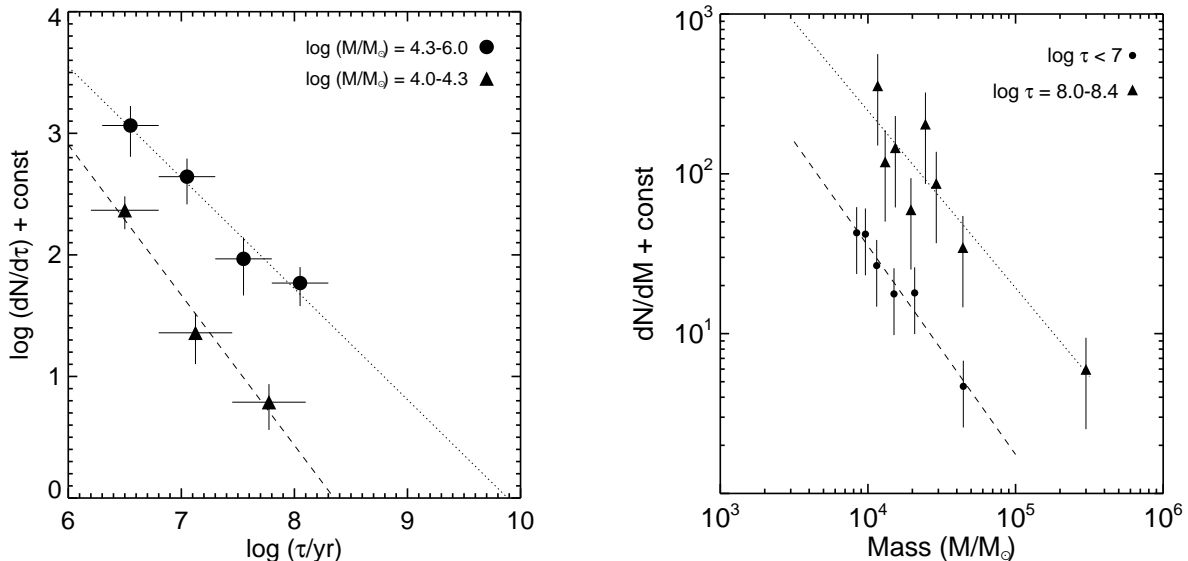


Figure 7. The age distribution of clusters in NGC 4449 in the indicated intervals of mass is shown on the left, and the mass function in the indicated intervals of age is shown on the right. The lines show the best fits to the distributions. See text for more details.

ies, including dwarf irregular, spiral, and merging galaxies. All of these different galaxies appear to have similar shapes to their (mass-limited) age distributions, where they decline from the present to the past (over the past $\approx \text{few} \times 10^8 - 10^9$ yr). This shape for the age distribution has previously been interpreted as due primarily to the gradual, early disruption rather than to the formation of the clusters, since it is far more likely that the clusters in all of these galaxies have similar disruption histories than it is that they have similar formation histories.

After their formation in the dense cores of giant molecular clouds, different physical processes cause clusters to lose mass and to eventually disrupt. Fall et al. (2009) and Chandar et al. (2010a) have suggested the following approximate sequence and timescale for these processes: (1) removal of ISM by stellar feedback, $\tau \lesssim 10^7$ yr; (2) continued stellar mass loss, $10^7 \text{ yr} \lesssim \tau \lesssim 10^8$ yr; and (3) tidal disturbances by passing molecular clouds, $\tau \gtrsim 10^8$ yr. It is likely that the cluster mass and age, which can be approximated by power-law distributions, result from a complex situation that involves several of these disruption processes. We refer the interested reader to Fall et al. (2009) and Chandar et al. (2010a) for more details. On longer timescales, mass-loss is driven by the escape of stars due to internal two-body relaxation, or evaporation.

5. SPATIAL CORRELATION BETWEEN X-RAY AND OPTICAL SOURCES

5.1. Correlation Between the Positions of XRBs and Star Clusters

Kaaret et al. (2004) previously suggested that X-ray sources in three different starburst galaxies (M82, NGC 1569 and NGC 5253) may have formed in young star clusters, because they are preferentially located near star clusters, albeit with a significant displacement (≈ 200 pc on average). This conclusion was based on a comparison between the cumulative distribution of displacements measured between actual X-ray sources and their closest

clusters, and simulated displacements from a population of X-ray sources distributed randomly relative to the clusters. In order to explore whether or not X-ray binaries form in compact star clusters, here we compare the positions (of the entire sample) of 23 candidate X-ray binaries (presented in Section 2) with those of the star clusters (Section 3), to look for a statistically significant spatial correlation between the two.

We repeat the spatial correlation analysis performed by Kaaret et al. (2004) for our sources in NGC 4449. We identify the nearest star cluster to each X-ray binary, and measure the (projected) distance between the two. For XRBs that are not coincident with clusters, this gives a lower bound on the displacement of the source from its parent cluster, since the closest cluster is not necessarily the parent. The results for NGC 4449 are shown in Figure 8 as a cumulative distribution of the separations between the binaries and the closest cluster. The figure shows that there are 7 XRBs that are within 100 pc of a star cluster, and nearly all are within ≈ 400 pc of a star cluster. Interestingly, three HMXBs in NGC 4449 are spatially *coincident* with very young star clusters (within the 1σ positional uncertainty of $\approx 0.5''$ for *Chandra*), suggesting that these XRBs formed within the clusters.

To determine whether the clustering of XRBs near star clusters is statistically significant, we compare the observations with simulated X-ray source populations. We consider two different randomly distributed cases, i.e. where the X-ray sources are *not* associated with the clusters. First, we generate random sets of (23) uniformly distributed sources, as done in Kaaret et al. (2004), and find spatial displacements from the star clusters using the procedure described above. The simulation was run 1000 times, with the cumulative distribution determined in exactly the same way as for the actual observations, and the median result shown as the blue line in Figure 8. The uniformly distributed random sources show a clear difference from the observed spatial displacements, similar to the results found by Kaaret et al. (2004) for three different starburst galaxies (not including NGC 4449).

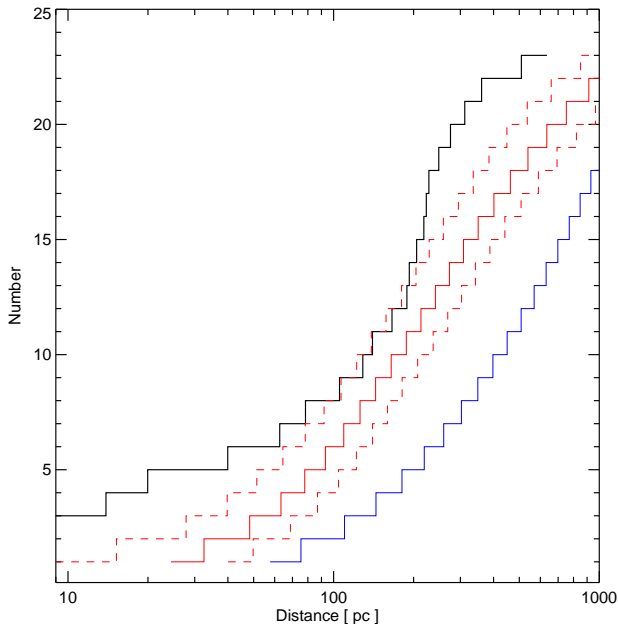


Figure 8. Cumulative distribution of the displacement (in parsecs) between X-ray binaries and star clusters. The black (solid) line shows the result for sources in NGC 4449. The other lines show results from our Monte Carlo simulations. The red solid line is the median of 1000 random distributions where the locations of the X-ray sources are drawn from a distribution that follows the light of the galaxy. The dashed lines show the 1σ deviation from this median curve. The blue solid line represents the median of 1000 random distributions where the X-ray source locations are drawn randomly from across the face of the galaxy.

Next, we select random sets of (23) sources distributed in a more realistic fashion, one where the XRBs fall off radially like the stellar light in NGC 4449 itself. This was accomplished by fitting the radial luminosity profile of NGC 4449 in a 2MASS K band image, by a broken power-law, $\phi(L) \propto L^\alpha$, with $\alpha = -0.79$ over the radial range $150 - 800$ pc, and $\alpha = -2.28$ over the radial range $800 - 3000$ pc. The K band should give a reasonably good measure of the distribution of older stars that form the stellar backbone of NGC 4449, rather than the distribution of young star clusters. The median result from 1000 runs of the random simulations described above are shown as the solid red line in Figure 8. In this case, the results of the randomly drawn spatial displacements are more similar to the observations, except at the small displacement end, with the observations now overlapping partly with the 1σ uncertainty line from the simulation at separations $\gtrsim 100$ pc. We find that a radial profile of NGC 4449 determined from far-ultraviolet images taken with GALEX gives very similar results to those based on the K -band profile. Our results indicate that the specific recipe used to populate synthetic X-ray sources in the image can affect the interpretation of the results, i.e. whether or not the X-ray sources are associated with star clusters. In general, a uniform distribution is much more likely to place synthetic X-ray sources in the outer portions of the galaxy when compared with the second method; because there are few X-ray sources located in the outskirts of NGC 4449, this procedure causes the simulation and observations to look substantially different.

We conclude that, in the case where the sources are distributed randomly but in a fashion similar to the underlying galaxy light, the random distribution does not differ significantly from the observed one, *except* at the smallest separations, where we find several XRBs closer to star clusters than predicted by the random distributions. These sources are discussed in more detail in Section 6.

5.2. Optical Sources That are Coincident With HMXBs

Three of the candidate HMXBs (X12, X21 and X46) have young ($\tau \lesssim 10^7$ yr) star clusters located within their $\approx 0.5''$ positional uncertainties. There is also an XRB coincident with an old globular cluster (X29); this is almost certainly a low-mass X-ray binary (LMXB). Here, we check the probability that this spatial coincidence is due to chance superposition rather than to a physical association between the HMXBs and the clusters. We distribute 23 XRBs (the number in our sample) randomly throughout NGC 4449 in 100,000 runs, and find one chance superposition approximately every fifth run when all 129 clusters were included. This is ≈ 25 times less than the four real observed coincidences between star clusters and XRBs. The probability of a chance superposition is almost identical if we only consider the three coincident HMXBs and star clusters younger than 10 Myr, i.e. the most probable host clusters. Here, the random sources follow the luminosity profile of NGC 4449 (see Section 4.1). If the random sources are uniformly distributed instead, we find coincidences only $\sim 3\%$ of the time, approximately 1 out of every 30 runs. Our results indicate that the positional coincidence between the XRBs and clusters in these three cases has a high statistical significance, and it is highly unlikely the result of chance superposition.

In addition to the XRBs that are coincident with star clusters, several others are coincident with an optical point source: X6, X10, X14, X20, and X24, as presented in Section 3.2. These point sources are well within the body of NGC 4449. They have the colors and magnitudes expected of supergiant stars, and are almost certainly the donor star in the X-ray emitting binary. Other candidate HMXBs are located in crowded regions, making it more difficult to identify a unique optical counterpart to the XRB, because there are several sources in the *HST* image within the positional uncertainties of the X-ray source. Some of the X-ray sources (e.g., X18, X13, X20, X11, and X19) do not have any obvious optical counterpart.

6. DISCUSSION

6.1. Properties of Star Clusters Closest to HMXBs

The ages of star clusters in the vicinity of the X-ray binaries can help to constrain the ages and the nature of the HMXBs. Even when there is no unambiguous stellar or cluster counterpart to an X-ray source, it is plausible that the XRB is the same age as the stars and clusters around it. Here, we present the physical properties of the star cluster that is closest to each HMXB. In Table 6, for each HMXB we compile the distance to the closest star cluster in our catalog, and the age and mass of this cluster. We also include the X-ray luminosity of each

source determined in Section 2.1, and a column that lists whether the X-ray colors are better described by a disk black body or a power law model, or are in the absorbed portion of the diagram.

The colors of HMXBs can vary, because these binaries go through different emission states, or because of their geometric orientation, since inclination effects through a disk can result in colors in the absorbed portion of the X-ray two-color diagram. This means that it is not possible to definitively identify the type of HMXB (e.g., black hole vs. neutron star) or to determine its age, just from the X-ray properties. However, different types of HMXBs do show some general trends in the color-color diagram. For example, black hole binaries often approximately follow the disk black-body models (Remillard & McClintock 2006). At high accretion rates the X-ray emission from black hole binaries is dominated by thermal emission from a disk, leading to both high luminosities and soft X-ray colors. On the other hand, accreting low-mass neutron star binaries often have absorbed power-law spectra.

6.2. A Population of Very Young, Massive Black Hole Binaries in NGC 4449

We can select very young binaries, which are likely to be high-mass black hole binaries (BHB), in two different ways: (1) from their location in the X-ray color-color diagram, and (2) from their proximity to very young star clusters. We first select candidate BHBs from Table 6 based on their X-ray colors. There are seven X-ray sources that are best described by disk black-body models: X12, X21, X23, X24, X28, X42 and X46. All of these X-ray sources are either coincident with (X12, X21, and X46), or fairly close to (within 200 pc) a very young $\tau \lesssim 8$ Myr star cluster.⁸ The coincidence with clusters is particularly important, because it establishes a direct connection between the BHBs and very young clusters (recall that in Section 5.1 we found that chance superpositions are highly unlikely). These seven sources have a median X-ray luminosity of 2.25×10^{37} erg s⁻¹. The fact that they have the X-ray colors expected for BHBs and are also close to very young star clusters strongly supports that these sources are in fact, very young BHBs (discussed in more detail below).

Next, we select candidate black hole binaries based solely on their proximity (within 200 pc) of a very young ($\tau \lesssim 8$ Myr) star cluster. These criteria return all seven XRBs described by the disk black body models, plus four additional sources: X6, X22, X43, and X44. All four of these are found in the “absorbed” portion of the X-ray two-color diagram. However, they are located near star forming regions which contain very young $\tau \lesssim 8$ Myr star clusters, and that are further out in NGC 4449 (with galactocentric distances $R_g \gtrsim 1.2$ kpc) on average than the seven sources discussed previously. The stellar density of the galaxy has dropped significantly at these galactocentric distances, which strongly suggests that X6, X22, X43, and X44 are associated with the nearby, recent star formation. In fact, random simulations return only a single XRB with $R_g \gtrsim 1.2$ kpc and

within 200 pc of a young star cluster in 10,000 runs.

The physical association between BHBs and very young star clusters is also apparent as the small separations in the cumulative distribution of spatial displacements between XRBs and star clusters (Figure 8). This regime deviates strongly from random distributions, as we would expect if BHBs are physically associated with very young star clusters. We conclude that (at least some) BHBs form in, and not just near, compact star clusters, based on the fact that three candidate BHBs in our sample are spatially coincident with a very young star clusters and that a fourth is very close to a young cluster (within a projected distance of 13 pc).

The ages of $\tau \lesssim 6 - 8$ Myr estimated for the coincident and proximate star clusters to the 11 XRBs discussed above strongly suggests that these are black hole (rather than neutron star) binaries. At these very young ages, only stars initially more massive than $M \gtrsim 25 - 30 M_\odot$ will have had time to become supernovae (based on the Padova models for solar metallicity). While there is still some uncertainty about the exact range of stellar masses that end their lives as black holes rather than as neutron stars, most models predict that the transition between these two types of compact remnants occurs for star with initial masses somewhere in the range of $\approx 18 - 25 M_\odot$ (e.g., Fryer (1999)), below the initial stellar masses that have completed their main sequence lifetime in $\approx 6 - 8$ Myr old star clusters. However, metallicity effects may complicate the relationship between initial stellar mass and remnant type (e.g., Heger et al. (2003)). Given these uncertainties we will refer to these as ‘candidate’ BHBs.

One of the XRBs that is best described by a disk black-body model, X24, is not coincident with a star cluster, but is coincident with a bright point source. The lack of any other bright stars within the 1σ astrometric uncertainty suggests that this is the high mass donor star in the XRB. The luminosity and color of this source are consistent with isochrones that are $\approx 8 - 10$ Myr, as shown in Figure 4, similar to the age of the nearest star cluster.

To summarize, the main results of this section are that we find strong evidence for a population of BHBs in NGC 4449, and that these massive binaries likely formed recently in compact star clusters. Three of the candidate BHBs appear to reside within their parent star clusters, while the others do not. These very young ($\tau \lesssim 6 - 8$ Myr) sources comprise a significant fraction of all X-ray emitting binaries brighter than $\approx \text{few} \times 10^{36}$ erg s⁻¹ in NGC 4449. BHBs therefore make up approximately 48% or 11 out of 23 XRBs.

6.3. Processes Responsible for the Spatial Displacement Between BHBs and Star Clusters

Black holes are the compact remnants of massive O stars. O stars typically form in (massive) clusters rather than in the field, although they can be dynamically ejected from clusters into the field. For example, studies of field O stars in the Milky Way (de Wit et al. 2005) show that the majority of field O stars appear to be runaways from nearby star clusters. Moreover, many and possibly most O stars are born in binaries (García & Mermilliod 2001; Larson 2001). Section 6.2 provided strong evidence that BHBs probably form in

⁸ Source X21 also happens to have an older, $\tau \approx 200$ Myr cluster nearby.

Table 6
Properties of Star Cluster Closest to XRBs in NGC 4449

ID	X-ray Model	ID of Closest Cluster	Cluster Age ¹ log(τ /yr)	Distance (pc)	Notes
X8	Absorption	96	9.34	266	
X14	Absorption	117	8.06	339	
X18	...	117	8.06	285	
X13	Absorption	112	8.06	232	
X6	Absorption	93	6.64	122	
X29	...	89	8.91	7	LMXB
X10	Power-law	99	8.31	286	
X12	Disk blackbody	104	6.96	10	Coincident
X20	Absorption	33	8.86	222	
X11	Absorption	102	8.36	89	
X23	Disk blackbody	66	6.58	181	
X15	Power law	13	8.31	9	Coincident
X24	Disk blackbody	69	6.84	68	
X21	Disk blackbody	53	6.72	13	Coincident
X28	Disk blackbody	81	6.72	136	
X31	...	87	6.70	630	
X22	Absorption	70	6.38	133	
X19	Super soft source	51	8.06	383	
X41	Super soft source	50	6.90	225	
X42	Disk blackbody	6	6.40	113	
X43	Absorption	62	6.40	57	
X44	Absorbed	75	6.16	134	
X46	Disk blackbody–Power law	111	6.70	4	Coincident

¹ Uncertainties in the cluster age estimates are typically ± 0.3 in log τ .

star clusters.

In the previous section, we found that while three of the candidate BHBs in NGC 4449 are coincident with a star cluster, the majority of them are not. What physical process(es) is responsible for this displacement between BHBs and their parent clusters? We consider three different mechanisms that could lead to the apparent displacement between BHBs and their parent star clusters:

- The parent cluster has dissolved and is therefore no longer visible, leading to an apparent displacement between the BHB and neighboring clusters.
- The BHB was ejected from its parent cluster during dynamical interactions with stars in the dense cluster core (Poveda et al. 1967; Gies & Bolton 1986).
- The BHB was ejected from its parent cluster due to an asymmetric supernova kick (Zwicky 1957; Blaauw 1961).

In Section 4, we suggested that the shape of the cluster mass and age distributions in NGC 4449 are primarily signatures of the disruption rather than the formation of the clusters. Regardless of whether individual clusters dissolve partially or fully, our results in NGC 4449 (and those in other galaxies), suggest that star clusters lose a significant amount of mass very quickly, on timescales of only ≈ 10 Myr.⁹ UV spectra of starburst galaxies reveal that the dispersed field populations are dominated by B stars, whereas UV-bright star clusters are often dominated by O stars, consistent with a scenario of rapid

cluster dispersal and/or mass-loss (e.g., Tremonti et al. (2001); Chandar et al. (2003)). Despite growing evidence that even massive star clusters, i.e., those most likely to host O stars, may disperse rapidly, we believe that this is unlikely to be the mechanism responsible for the observed spatial displacement between very young BHBs and star clusters. N-body simulations show that an unbound cluster retains the appearance of a bound cluster for 10 – 20 crossing times (Baumgardt & Kroupa 2007), on the order of 10-20 Myr for typical clusters in our NGC 4449 catalog. Since no cluster is observed at the locations of the majority of the BHBs, the early dispersal of clusters can be ruled out as the origin of the spatial displacement between very young, high mass BHBs and star clusters.

We conclude that many BHBs in NGC 4449 have been ejected from their parent clusters, either via dynamical kicks due to interactions with other stars in cluster cores, or due to an asymmetry in the supernova explosion of the compact object, which nonetheless does not unbind the binary. We cannot differentiate between these two mechanisms using the current observations. We can however, estimate lower and upper limits to the ejection velocities. We estimate a lower kick velocity by assuming that each BHB was ejected from its closest cluster very soon after it formed, and divide the distance to this cluster by its age, neglecting for the moment uncertainties in the cluster age estimates. These lead to lower limits of 45, 10, 27, and 23 km/s for X23, X24, X28, and X42, respectively. The other BHB binaries give limits of 28, 55, 23, and 84 km/s for X6, X22, X43, and X44. The cluster ages and hence the velocities are uncertain by \approx a factor of two, resulting in lower limits to the velocities between $\approx 5 - 160$ km/s. Of course dynamical ejection need not have occurred right after the cluster formed, but could have occurred more recently. We estimate upper limits to the kick velocities by assuming that each BHB was

⁹ This early mass loss is not driven by relaxation of the cluster due to two-body interactions (e.g., Fall & Zhang (2001)). Relaxation-driven evaporation operates on significantly longer timescales than the ages of the BHBs, and ejects mostly low mass stars.

ejected within the last 1 Myr, i.e. we divide the distance by 1 Myr. This procedure gives a range of velocities (for non-coincident sources) between $\approx 30 - 180$ km/s.

6.4. The Nature of Older X-ray Binaries in NGC 4449

In the previous subsections we found that ≈ 11 of the 23 candidate XRBs in NGC 4449 are likely very young, massive BHBs. The goal of this section is to better understand the ages and types of the remaining X-ray binaries.

We first constrain the number of low mass X-ray binaries (LMXBs) in NGC 4449, systems consisting of a black hole or neutron star accreting from a *low-mass* companion. Source X29 is almost certainly a LMXB, because it is spatially coincident with a cluster that has integrated colors similar to those of ancient Galactic globular clusters. Its X-ray colors and luminosity however, are unremarkable when compared with the rest of the XRB sample, and therefore cannot be used to select ancient LMXBs in general. In their study of five early-type galaxies (ellipticals and lenticulars), which have formed LMXBs but not HMXBs, Kundu et al. (2007) find $\approx 25 - 60\%$ of all LMXBs are coincident with globular clusters and the rest are found in the field. Assuming a similar fraction of cluster-to-field LMXBs in NGC 4449 implies that there are $\approx 2 - 4$ field and hence $\approx 3 - 5$ total LMXBs in NGC 4449, $\approx 13 - 22\%$ of our total sample.

Our analysis implies that there are 7 – 9 remaining X-ray binaries in NGC 4449 that are neither very young, high mass BHBs nor very old LMXBs. These are likely older than ≈ 10 Myr and younger than several billion years (age of LMXBs). Interestingly, from Table 6 we find that the closest clusters to X14, X18, X13, X10, X20, X11, and X19 are all intermediate age, with $\tau \approx 100 - 400$ Myr. The separations between these X-ray binaries and their closest clusters is larger than those found between BHBs and their closest clusters, with a median (mean) separation of ≈ 285 pc (250 pc).

These “intermediate” age HMXBs are likely neutron star X-ray binaries with either a Be or supergiant star for a companion. Accretion from the former occurs via a disk, while the latter are primarily wind fed. There are also differences in the optical luminosities of Be versus supergiant donor stars: Be-HMXBs in the Small Magellanic Cloud have M_V ranging from -2 to -5 (McBride et al. 2008), which at the distance of NGC 4449 corresponds to $m_V \approx 26 - 23$, while supergiant HMXBs in the Galaxy are significantly brighter (Chevalier & Ilovaisky 1998), with M_V brighter than ≈ -6.5 ($m_V \lesssim 21.5$). X10 and X14 are therefore candidate supergiant-HMXBs, because they have bright coincident point sources (see Section 3.2). X18, X13, X20, X11, and X19 however, do not show any bright coincident point sources in the optical images down to $m_V \approx 25$, and are therefore likely Be-HMXBs.

Be-X-ray binaries dominate the population of HMXBs in the Magellanic Clouds (McBride et al. 2008). They turn-on approximately 20-50 Myr after a star formation event, as the first neutron stars are formed. The low mass of the neutron star and lower accretion rates mean that Be-X-ray binaries typically have lower X-ray luminosities than massive BHBs. However, most Be star X-ray binaries go into outburst when the neutron star passes through the circumstellar disk of the Be star and the

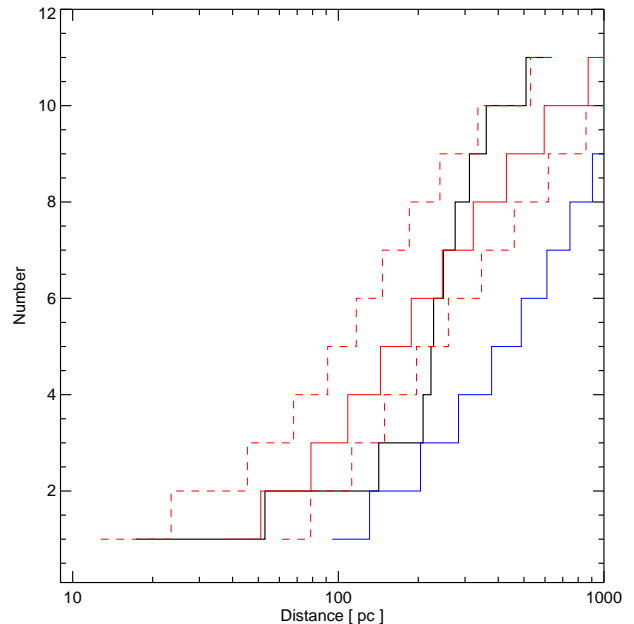


Figure 9. Same as Figure 8, but excluding the eleven massive BHBs and the known LMXB.

accretion rate increases. We note that the candidate Be-HMXBs in NGC 4449 have X-ray luminosities considerably higher than quiescent Be X-ray binaries. If they are indeed Be X-ray binaries, then they are in outburst, and we are detecting only the highest luminosity sources. This would suggest there is a much larger population of Be X-ray binaries in NGC 4449 below our detection threshold.

In Section 6.2 we used the spatial displacement diagram to support our conclusion that very young, massive BHBs form in compact star clusters. Here, we note that there is an inherent limitation in our ability to interpret this diagram for older binaries. While the association between very young clusters and XRBs shows up clearly, this is not true for intermediate age sources. Figure 9 shows the cumulative distribution of displacements between $\tau \gtrsim 10$ Myr X-ray binaries and star clusters, where we have removed the BHBs and the known LMXB. After $\approx 50 - 100$ Myr, XRBs that have been ejected at even low velocities of a few km/s are no longer obviously spatially associated with their parent clusters, since at separations larger than ≈ 200 pc the distribution is consistent with the 1σ uncertainties from a random distribution.

7. SUMMARY AND CONCLUSIONS

In this paper, we presented the discovery of 23 candidate X-ray binaries in the nearby starburst galaxy NGC 4449, from *Chandra*/ACIS-S observations. We measured count rates, luminosities, and colors for these sources.

We also presented a new catalog of 129 compact star clusters brighter than $M_V \approx -7$ in NGC 4449 from multi-band, high resolution, optical imaging taken with the ACS/WFC and WFPC2 cameras on-board the *HST*. This doubled the number of compact star clusters known in this galaxy. Mass and age estimates for these clusters show that NGC 4449 has formed relatively massive

($M \gtrsim 10^4 M_\odot$) clusters more or less continuously over the last $\approx 10^9$ yr. The joint distribution of cluster ages and masses appears to be similar to those found in other nearby galaxies such as the Magellanic Clouds, M83, and the merging Antennae galaxies, albeit with somewhat larger uncertainties due to the smaller number of clusters, and can be approximated as $g(M, \tau) \propto M^\beta \tau^\gamma$, with $\beta = -2.16 \pm 0.30$ and $\gamma = -1.0 \pm 0.3$.

Our main conclusion is that we have found clear evidence for a population of very young, high mass, black hole X-ray binaries in NGC 4449. We find 11 candidate high mass BHBs, nearly half of the sample of X-ray emitting binaries. Three of the BHB candidates are coincident, within the astrometric uncertainties of *Chandra*, with a very young, $\tau \lesssim 8$ Myr star cluster, and a fourth is nearly coincident with a very young cluster. The others are all within 200 pc of very young clusters. Based on these results, we suggest that these massive BHBs form in star clusters, where most massive O stars (the progenitors of BHBs) are born. Many are subsequently ejected from their parent clusters either due to dynamical interactions within dense clusters or as the result of an asymmetric supernova explosion. The observed displacement between BHBs and very young star clusters is not caused by the dissolution of the parent clusters. The small separation between massive BHB candidates and their closest cluster clearly deviates from randomly populated distributions, further supporting our conclusion that these X-ray binaries have a direct relationship with young star clusters.

We found one X-ray binary in NGC 4449 that is coincident with an old star cluster, and hence is almost certainly a LMXB. Based on the fraction of LMXBs found in the field vs. in globular clusters in early-type galaxies, we estimate that there are $\approx 2 - 4$ field LMXBs and hence 3 – 5 total LMXBs in NGC 4449, although they cannot be identified from their X-ray properties alone.

We suggest that the remaining XRBs are intermediate age supergiant and Be-HMXBs. Although none of these remaining binaries are coincident with a star cluster, the closest cluster to these sources has an estimated age between 100–400 Myr. In two cases, we identify coincident point sources in the *HST* images that have luminosities consistent with those expected of supergiant donor stars. The other candidate intermediate-age X-ray binaries do not have an obvious optical counterpart, consistent with the expected luminosities for Be star donors.

Based on these results, we conclude that high mass X-ray binaries, particularly massive, black-hole binaries, dominate the X-ray luminosity from NGC 4449. We suggest that the ages and locations of star clusters provide important insight and constraints on the different types of X-ray binaries in nearby star-forming galaxies.

We thank the anonymous referee, whose careful reading and helpful suggestions significantly improved our

manuscript. This work was supported by NASA contract NAS8-39073 (CXC) and NASA AR8-9010.

REFERENCES

- Annibali, F., Aloisi, A., Mack, J., Tosi, M., van der Marel, R. P., Angeretti, L., Leitherer, C., & Sirianni, M. 2008, *AJ*, 135, 1900
- Baumgardt, H., & Kroupa, P. 2007, *MNRAS*, 380, 1589
- Blaauw, A. 1961, *Bull. Astron. Inst. Netherlands*, 15, 265
- Bruzual, G., & Charlot, S. 2003, *MNRAS*, 344, 1000
- Chandar, R., Leitherer, C., Tremonti, C., & Calzetti, D. 2003, *ApJ*, 586, 939
- Chandar, R., Fall, S. M., & Whitmore, B. C. 2010, *ApJ*, 711, 1263
- Chandar, R., et al. 2010, *ApJ*, 719, 966
- Chandar, R., Whitmore, B. C., & Fall, S. M. 2010, *ApJ*, 713, 1343
- Chevalier, C., & Ilovaisky, S. A. 1998, *A&A*, 330, 201
- de Wit, W. J., Testi, L., Palla, F., & Zinnecker, H. 2005, *A&A*, 437, 247
- Dolphin, A. 2000, *PASP*, 112, 1397
- Fall, S. M., Chandar, R., Whitmore, B. C. 2005, *ApJ*, 631, 133
- Fall, S. M., Chandar, R., Whitmore, B. C. 2009, *ApJ*, 705, 453
- Fall, S. M., Krumholz, M. R., & Matzner, C. D. 2010, *ApJ*, 710, L142
- Fall, S. M., & Zhang, Q. 2001, *ApJ*, 561, 751
- Fitzpatrick, E. L. 1999, *PASP*, 111, 63
- Freeman, P. E., Kashyap, V., Rosner, R., & Lamb, D. Q. 2002, *ApJS*, 138, 185
- Fryer, C. L. 1999, *ApJ*, 522, 413
- García, B., & Mermilliod, J. C. 2001, *A&A*, 368, 122
- Gelatt, A. E., & Hunter, D. A., & Gallagher, J. S. 2001 *PASP*, 113, 142
- Gies, D. R., & Bolton, C. T. 1986, *ApJS*, 61, 419
- Girardi, L., Dalcanton, J., Williams, B., et al. 2008, *PASP*, 120, 583
- Grevesse, N., & Sauval, A. J. 1998, *Space Sci. Rev.*, 85, 161
- Heger, A., Fryer, C. L., Woosley, S. E., Langer, N., & Hartmann, D. H. 2003, *ApJ*, 591, 288
- Holtzman, J., Burrows, C. J., Casertano, S., Hester, J., Trauger, J. T., Watson, A. M., & Worthey, G. 1995a, *PASP*, 107, 1065
- Hunter, D. 1997, *PASP*, 109, 937
- Kaaret, P., Alonso-Herrero, A., Gallagher, J. S., Fabbiano, G., Zezas, A., Rieke, M. J. 2004, *MNRAS*, 348, 28
- King, I. R. 1966, *AJ*, 71, 64
- Kundu, A., Maccarone, T. J., & Zepf, S. E. 2007, *ApJ*, 662, 525
- Larsen, S. 1999, *A&AS*, 139, 393
- Larson, R. B. 2001, *The Formation of Binary Stars*, 200, 93
- Liedahl, D. A., Osterheld, A. L., & Goldstein, W. H. 1995, *ApJ*, 438, L115
- Marigo, P., Girardi, L., Bressan, A., et al. 2008, *A&A*, 482, 883
- McBride, V. A., Coe, M. J., Negueruela, I., Schurch, M. P. E., & McGowan, K. E. 2008, *MNRAS*, 338, 1198
- McSwain, M. V., Ransom, S. M., Boyajian, T. S., Grundstrom, E. D., Roberts, Mallory S. E. 2007, *ApJ*, 660, 740
- Mitsuda, K., et al. 1984, *PASJ*, 36, 741
- Patnaude, D. J., Fesen, R. A. 2003, *ApJ*, 587, 221
- Poveda, A., Ruiz, J., & Allen, C. 1967, *Boletín de los Observatorios Tonantzintla y Tacubaya*, 4, 86
- Prestwich, A. H., Irwin, J. A., Kilgard, R. E., Krauss, M. I., Zezas, A., Primani, F., & Kaaret, P., & Boroson, B. 2003, *ApJ*, 595, 719
- Remillard, R. A. & McClintock, J. E. 2006, *ARA&A*, vol. 44, Issue 1, pp.49-92
- Sirianni, M., M.J. Jee, N. Bentez, J.P. Blakeslee, A.R. Martel, G. Meurer, M. Clampin, G. De Marchi, H.C. Ford, R. Gilliland, G.F. Hartig, G.D. Illingworth, J. Mack, and W.J. McCann 2005, *PASP*, 117, 1049
- Thronson, H. A., Jr., Hunter, D. A., Telesco, C. M., Decher, R., & Harper, D. A. 1987, *ApJ*, 317, 180
- Tremonti, C. A., Calzetti, D., Leitherer, C., & Heckman, T. M. 2001, *ApJ*, 555, 322
- Whitmore, B. C., Chandar, R., & Fall, S. M. 2007, *AJ*, 133, 1067
- Zezas, A., Fabbiano, G., Rots, A. H., Murray, S. S. 2002, *ApJ*, 577, 710
- Zwicky, F. 1957, Berlin: Springer, 1957